Mixed pinning landscape in nanoparticle-introduced $YGdBa_2Cu_3O_y$ films grown by metal organic deposition

M. Miura,[1,*] B. Maiorov,[1] S. A. Baily,[1,2] N. Haberkorn,[1] J. O. Willis,[1] K. Marken,[1] T. Izumi,[3] Y. Shiohara,[3] and L. Civale[1]

[1]*Superconductivity Technology Center, Los Alamos National Laboratory, Los Alamos, New Mexico 87545, USA*

[2]*National High Magnetic Field Laboratory, Los Alamos National Laboratory, Los Alamos, New Mexico 87545, USA*

[3]*Superconductivity Research Laboratory, International Superconductivity Technology Center, 10-13, Shinonome 1-chome, Koto-ku, Tokyo, 135-0062, Japan*

(Received 2 November 2010; published 25 May 2011; corrected 3 June 2011)

We study the field (**H**) and temperature (T) dependence of the critical current density (J_c) and irreversibility field (H_{irr}) at different field orientations in $Y_{0.77}Gd_{0.23}Ba_2Cu_3O_y$ with randomly distributed $BaZrO_3$ nanoparticles (YGdBCO + BZO) and $YBa_2Cu_3O_y$ (YBCO) films. Both MOD films have large $RE_2Cu_2O_5$ (225) nanoparticles (~80 nm in diameter) and a high density of twin boundaries (TB). In addition, YGdBCO + BZO films have a high density of BZO nanoparticles (~25 nm in diameter). At high temperatures ($T > 40$ K), the superconducting properties, such as J_c, H_{irr}, and flux creep rates, are greatly affected by the BZO nanoparticles, while at low temperatures the superconducting properties of both the YBCO and YGdBCO + BZO films show similar field and temperature dependencies. In particular, while the J_c of YBCO films follow a power-law dependence ($\propto H^{-\alpha}$) at all measured T, this dependence is only followed at low T for YGdBCO + BZO films. As a function of T, the YGdBCO + BZO film shows $J_c(T,0.01T) \sim [1-(T/T_c)^2]^n$ with $n \sim 1.24 \pm 0.05$, which points to "δT_c pinning." We analyze the role of different types of defects in the different temperature regimes and find that the strong pinning of the BZO nanoparticles yields a higher H_{irr} and improved J_c along the c axis and at intermediate orientations at high T. The mixed pinning landscapes due to the presence of disorder of various dimensionalities have an important role in the improvement of in-field properties.

DOI: 10.1103/PhysRevB.83.184519 PACS number(s): 74.25.Wx, 74.72.−h, 74.25.Sv

I. INTRODUCTION

Epitaxial films of the $REBa_2Cu_3O_y$ (REBCO, RE: rare-earth) family have the highest critical current density (J_c) of any known superconductor. For very thin films (~200 nm), at liquid He temperature and zero applied fields J_c's in the range of 80 to 100 MA/cm^2 have been reported.[1,2] This is more than a factor of 2 higher than in the superconductor with the next best J_c (Nb-Ti) and about 25 to 30% of the upper limit set by the depairing current density (J_0). However, although extremely high values of J_c and irreversibility (H_{irr}) and upper critical fields (H_{c2}) are possible at low temperature, as the temperature increases, J_c is reduced drastically in the presence of an applied field (**H**) until $J_c = 0$ at H_{irr}. Thus, increasing our fundamental knowledge of vortex pinning in this extreme case has a broader impact beyond these particular compounds and helps to improve the general understanding of vortex physics. On the other hand, the REBCO films are the core of the second-generation high-temperature superconductor (HTS) wires (also known as coated conductors), so this topic also has large technological relevance. In particular, studying and increasing the H_{irr} is critical to enhancing J_c at high fields.

Early analyses of vortex dynamics in HTS focused mostly on simple pinning landscapes defined by one type of defect, namely uncorrelated disorder produced by random point defects (i.e., of atomic size) and correlated disorder produced by columnar or planar defects. Elegant and sophisticated theoretical frameworks were developed for both cases.[3] Irradiations with light ions[4] and high-energy heavy ions[5] were extensively used to controllably introduce random point defects and columnar defects, respectively. Significantly less attention was devoted to the study of vortex matter in the presence of randomly distributed nanoparticles, i.e., second-phase inclusions with physical dimensions similar to or larger than the size of the vortex core, with the exception of the analysis of pinning by Y_2BaCuO_5 and other precipitates in melt-textured bulk YBCO.[6,7]

More recently, it became increasingly apparent that randomly distributed nanoparticles are key players in the strong vortex pinning in REBCO films.[8–12] Although much needed theoretical understanding is now being developed,[13,14] many important issues remain unknown, such as the influence of strong pinning centers on the nature of the vortex solid-liquid phase transition and the properties of the liquid phase. Furthermore, the microstructure of the REBCO films is quite complex with a proliferation of defects of various sizes, shapes, and compositions, all of which can, in principle, contribute to vortex pinning. Although the deconvolution of the contributions to J_c of different types of pinning centers is a very appealing idea, in general, the pinning effects of the various components in a mixed pinning landscape cannot be simply added. Synergistic effects among the disorder subsystems can play a large and indeed beneficial role, as in the combined effect of splayed columnar defects (nanorods) and random nanoparticles in the BZO-doped REBCO films grown by pulsed laser deposition (PLD),[15] or in single crystals with both random and columnar defects produced by combined proton and heavy ion irradiations.[16] A deeper and more quantitative understanding of the effects of complex pinning landscapes on J_c in particular and on the behavior of vortex matter in general is necessary for assessing the potential of coated conductors for high temperature and field applications, and to that end it is important to explore systems with well-controlled pinning landscapes.

In this work, we study the effect of various combinations of hybrid artificial dimensional disorder on H_{irr} up to 60 T and on the field and temperature dependence of J_c. To elucidate the influence of randomly distributed nanoparticles we have engineered microstructures with well-defined pinning landscapes using $BaZrO_3$ nanoparticle dispersed $Y_{0.77}Gd_{0.23}Ba_2Cu_3O_y$ (YGdBCO + BZO) grown by metal organic deposition (MOD). In order to single out the effects of the nanoparticles we extensively compare and contrast the vortex properties in this system with those in MOD $YBa_2Cu_3O_y$ (YBCO) films. We perform additional comparisons against two other systems without BZO nanoparticles, namely MOD $Y_{0.77}Gd_{0.23}Ba_2Cu_3O_y$ (YGdBCO) and PLD YBCO films. The analysis in these films is simplified by the fact that none of them contain second phase nanorods; however, we find that even undoped MOD YBCO possesses a significant density of large nanoparticles and that both the YGdBCO + BZO and MOD YBCO films have a large density of twin boundaries (TB), which act as correlated (planar) disorder. We compare the experimental results for J_c (T, H,Θ) and H_{irr} (T, Θ) with theoretical models and discuss the possibility of improvement of the critical current density.

II. EXPERIMENTAL DETAILS

We grew ~0.6-μm-thick films of YBCO and YGdBCO + BZO derived from the trifluoroacetate MOD process and grown on ion-beam-assisted deposition metal templates (IBAD).[17] We introduced Zr-naphthenate into organic solutions containing dissolved Y-, Gd-, and Ba-trifluoroacetates and Cu-naphthenate with the cation ratio of 0.77 : 0.23 : 1.5 : 3. The content of BZO in the films was 1 wt%, and the metal ion concentration of the starting solution was 1.2 mol/l. The details of the sample preparation have been published elsewhere.[18] The YBCO and YGdBCO + BZO films have a T_c of 89.9 and 90.5 K, and a J_c at 77 K, self-field of 3.0 and 4.1 MA/cm^2, respectively. For transport studies the films were patterned into bridges of width ~200 μm using standard photolithography. A standard four-terminal transport technique was used to measure the angular dependence of J_c in liquid nitrogen (77 K) and liquid neon (26 K), using a 1-μV/cm criterion. The resistivity (ρ) versus H measurements in pulsed fields were performed at the National High Magnetic Fields Laboratory at Los Alamos National Laboratory. A low AC current corresponding to 400 A/cm^2 at a frequency of 100 kHz was applied along the bridge. For pulsed fields, measurements at selected orientations (Θ) were performed by maintaining the sample at fixed angles. Additional ρ versus T measurements were performed in a dc magnet (Quantum Design Physical Property Measurement System) up to 14 T. H_{irr} was determined using a $0.01\rho_n$ criterion, where ρ_n is the normal state resistivity at the onset of the transition. In all transport studies the current was always perpendicular to **H** (maximum Lorentz force configuration). The magnetization data were obtained in a Quantum Design Magnetic Property Measurement System, and the critical current as a function of temperature and magnetic field was calculated using the Bean critical state model. The magnetic relaxation (flux creep) rate $S = d\log(J)/d\log(t)$ was determined by fitting the logarithmic decay of the magnetization as a function of time (t) over a 2-h period. The microstructure of the films was analyzed by transmission electron microscopy (TEM) using planar and cross-sectional views.

III. RESULTS AND DISCUSSION

A. The pinning landscape

There are a number of types of disorder of various dimensionalities that can act as pinning centers,[2] such as precipitates, TBs,[19] dislocations, point defects, nanorods,[15,20–22] nanoparticles,[9,10,23] and stacking faults. In this paper we show that TBs and nanoparticles are most relevant in our MOD films. The planar-view TEM of the MOD YBCO and YGdBCO + BZO films are shown in Figs. 1(a) and 1(b), respectively. Both films have large $RE_2Cu_2O_5$ (225) precipitates that remain in the MOD-REBCO layer when REBCO crystals are formed from the precursors containing BaF_2, $RE_2Cu_2O_5$, and CuO. The average density of these nanoparticles was found to be $n_{225} = 0.1 \times 10^{21}/m^3$ for both the YBCO and YGdBCO + BZO films and $n_{BZO} = 3.7 \times 10^{21}/m^3$ in the YGdBCO + BZO film. A particle-size distribution was extracted from high-magnification planar- and cross-section views (not shown) of several TEM images, and the results are shown in Figs. 1(c) and 1(d). The size of the 225 precipitates ranged from 74.4 to 100 nm with a modal particle size of 86.2 nm for both MOD films. The BZO nanoparticle size varied from 18 to 28 nm with a modal size of 23 nm. Taking $T_c = 90.5$ K, the average particle size matches the vortex core size ~2ξ(T) at $T_{BZO} = 90.35$ K, $T_{225} = 90.4$ K for ξ_{ab} and $T_{BZO} = 87.3$ K, $T_{225} = 90.3$ K for ξ_c. This indicates that even at high temperatures the BZO nanoparticles can act as strong pinning centers. From x-ray diffraction and selected-area diffraction pattern, we found that the lattice in most of the BZO nanoparticles is not coherent with the REBCO matrix.[24]

B. Critical current densities

Let us now consider the influence of various types of disorder on the critical current density J_c. In Fig. 2(a) we show the field dependence of $J_c(\mathbf{H}\|c)$ for the YBCO and YGdBCO + BZO films. We start with the YBCO film data. We find several common features observed in YBCO films grown by *in situ* and *ex situ* methods.[2,25] At low fields, J_c is nearly constant up to a characteristic crossover field B^*, followed by a power-law regime ($J_c \propto H^{-\alpha}$) at intermediate fields, observed as a linear dependence on the log-log plot. Finally, at the higher temperatures ($\geqslant$65 K) a more rapid decay of J_c is observed with H approaching the H_{irr}. The low-field regime can be associated with the single vortex pinning regime followed by a transition to pinning of interactive vortices at higher fields.[28]

Experimentally, the undoped YBCO films grown by PLD show $\alpha \sim 0.5$–0.6 depending on the amount of correlated pinning present, with $\alpha \sim 0.6$ in those films where weak pointlike defects dominate the pinning landscape.[2,25] For our MOD-YBCO film we find $\alpha \sim 0.60$–0.70. The value of α is consistently higher than that found for the PLD-YBCO film, an effect probably related to the lower density of c-axis-correlated dislocations in our MOD films. It has been shown that dislocations in MOD films do not connect from bottom to top

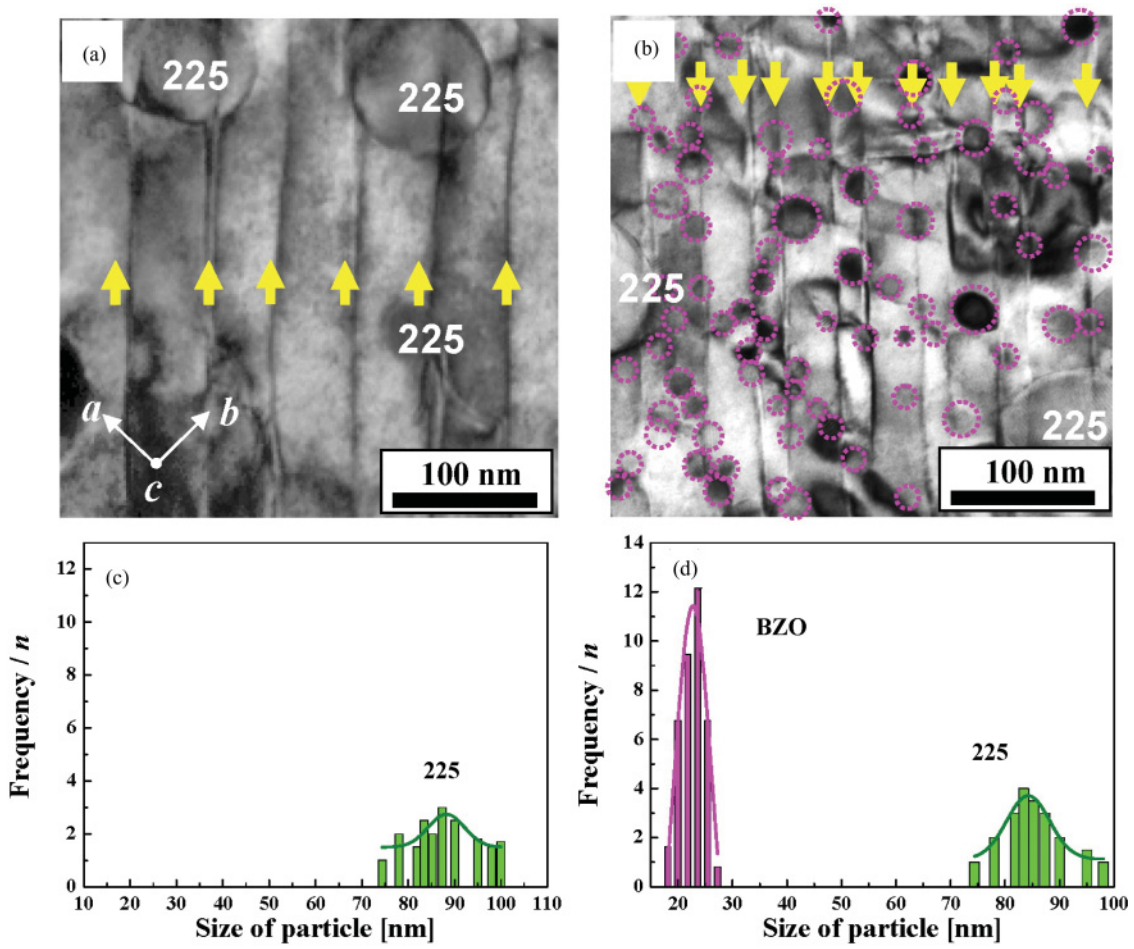

FIG. 1. (Color online) (a) High-magnification planar-view TEM image of the MOD YBCO CC showing TBs (yellow arrows) and large $Y_2Cu_2O_5$ (225) precipitates. (b) High-magnification planar-view TEM image of the MOD YGdBCO + BZO CC showing uniformly dispersed BZO nanoparticles (circles), TBs (yellow arrows), and 225 precipitates. [(c) and (d)] Histograms showing the distribution of particle size for YBCO and YGdBCO + BZO films, respectively. For comparison, the frequency is normalized by the density of nanoparticles, n.

due to lateral grain growth (grain boundary meandering)[12]; thus, they do not constitute c-axis-correlated disorder. This is also the case in our YBCO and YGdBCO + BZO films as seen using through-thickness atomic force microscope (AFM) visualizations obtained by etching the films (not shown). As seen in the inset table of Fig. 2(a), α values for the MOD-YBCO film do not change greatly with temperature, indicating a similar type of pinning throughout the entire temperature range. We can compare transport data at 77K for our MOD YBCO with an MOD YGdBCO film grown using the same procedures and investigated in Ref. 18. The YGdBCO film shows a slightly higher self-field J_c (3.7 MA/cm^2), a difference attributed to pinning by additional disorder due to the partial substitution of Gd in the Y site.[18] However, the field dependence in both cases is very similar, with almost identical α values (0.66 and 0.64 for MOD YBCO and YGdBCO, respectively), indicating that the pinning mechanisms are the same. It should be noted that the α values obtained from magnetization data at liquid N_2 temperatures are slightly higher than those obtained from transport measurements due to the much lower voltage criterion associated with the magnetically determined $J_c(H)$ as compared to transport measurements. (Due to the sharp I-V curves, $V \sim I^N$ with $N \gg 1$, the differences in α are negligible at low temperatures.) This issue was explored in detail by Thompson *et al.*,[26] and our own studies of this effect in several films are consistent with those results. In particular the different α values that we obtained for the MOD YBCO by transport and magnetization (at 77 K and 75 K respectively) are in agreement with the expectations.

We now turn our attention to the YGdBCO + BZO film. Figure 2(a) shows a significant enhancement in J_c for all temperatures and fields with respect to the YBCO film. Moreover, a clear increase in B^* is found for the YGdBCO + BZO film, consistent with the density and size of the BZO nanoparticles.[8,13]

Previous results in PLD films have shown that α depends both on the density and individual strength of c-axis-correlated defects and that the increased columnar pinning reduces α to values as low as 0.19.[15,25] This differs from what we found for the YGdBCO + BZO film at high temperatures, $T = 65$ and 75 K, where $J_c(H)$ does not follow a power-law dependence. However, this behavior of our YGdBCO + BZO film is similar to that observed in films with strong pinning coming from randomly dispersed nanoparticles of different chemical compositions (BZO or Y_2O_3) and growth methods

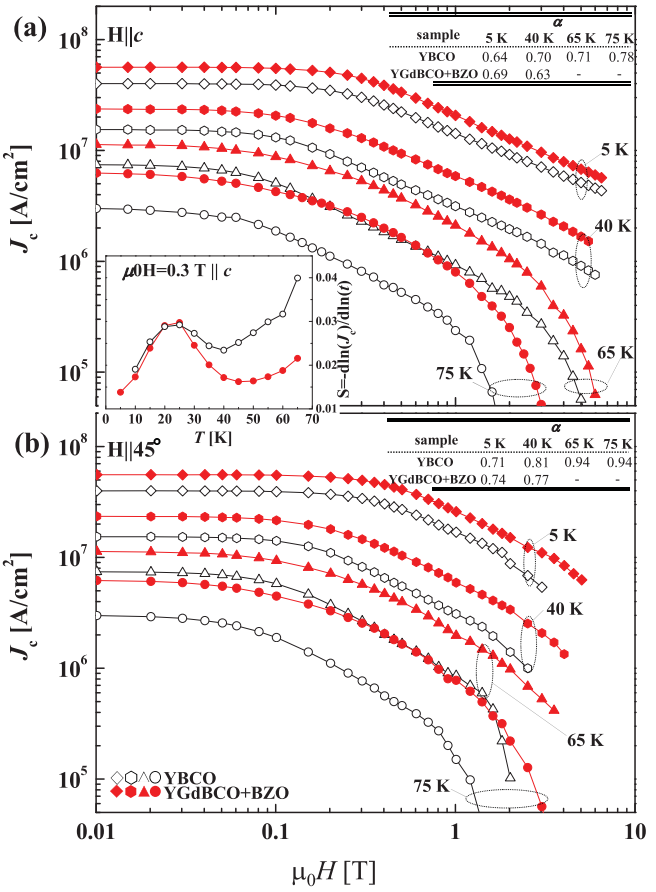

FIG. 2. (Color online) Comparison of magnetic field dependence of magnetization J_c curves for the YBCO (open symbols) and YGdBCO + BZO (solid symbols) films. The data are at various temperatures with the field applied parallel to (a) the c axis and (b) 45°. (Inset table) Power-law coefficient α at various temperatures for the YBCO and YGdBCO + BZO films at $\mathbf{H}\|c$ and $\mathbf{H}\|45°$, respectively. (Inset figure) The relaxation rate $S = -d\log(J)/d\log(t)$ versus T for YBCO (open symbols) and YGdBCO + BZO (solid symbols) films at $\mu_0 H = 0.3$ T $\|$ c axis.

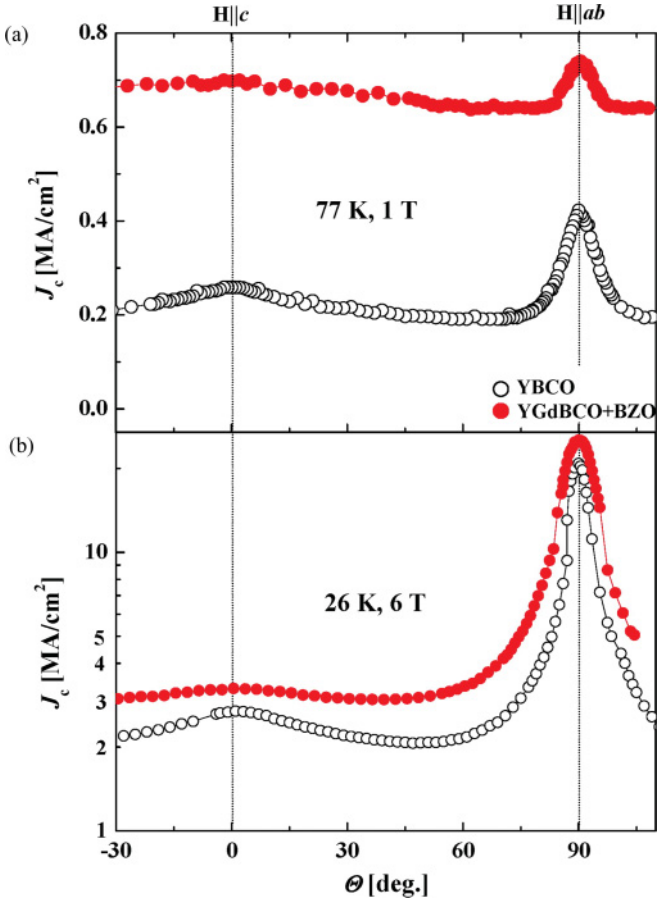

FIG. 3. (Color online) Angular dependence of J_c at (a) 77 K, 1 T and (b) 26 K, 6 T for the YBCO (open symbols) and YGdBCO + BZO (solid symbols) films.

(MOD or PLD).[9,10,14] As can be seen in Fig. 2, the non-power-law behavior in the YGdBCO + BZO is associated with a slow decay of J_c with field, making these films suitable for intermediate magnetic fields applications.

Figure 2(b) shows the field dependence of $J_c(\mathbf{H}\|45°)$ for the same YBCO and YGdBCO + BZO films shown in Fig. 2(a). In the YGdBCO + BZO film at high temperatures the power-law regime is also absent and the J_c values are very similar to those for $\mathbf{H}\|c$ [see Fig. 2(a)], indicating that the strong pinning of these nanoparticles extends over a wide angular range and is almost isotropic. This behavior is also confirmed by the nearly isotropic angular dependence of J_c at 77K shown in Fig. 3(a).

At low temperatures ($T \leqslant 40$ K), J_c in both the YBCO and YGdBCO + BZO films show a power-law dependence with similar α values. This is the case both for $\mathbf{H}\|c$ and $\mathbf{H}\|45°$ (see the tables in Fig. 2). It is also apparent that, even though the BZO nanoparticles clearly enhance J_c at all T, they are much less effective at low T. For instance, the ratio J_c(YGdBCO + BZO)/J_c(YBCO) at $\mu_0 H = 1$ T $\|c$ is 1.45 at 5 K, 2.28 at 60 K, and 3.39 at 75 K respectively, and the same trend is found if the ratio is taken at other values of H and/or for $\Theta = 45°$. A natural interpretation of this result is that pointlike randomly dispersed defects become more important at low T, due to the entropic renormalization of the pinning energy.[27–29] However, additional data indicate that the TBs also contribute to pinning in this temperature range. The first piece of evidence comes from $J_c(\Theta)$ at $T = 26$ K where a clear angular peak centered around the c axis is found in both samples, as shown in Fig. 3(b), even though the peak is less pronounced in the YGdBCO + BZO film due to the more isotropic additional pinning contribution of the BZO nanoparticles. Careful comparison of Figs. 2(a) and 2(b) also shows that at low temperatures and high fields $J_c(\mathbf{H}\|c) > J_c(45°)$, again hinting to some pinning contribution from TBs. Further evidence of the importance of TBs is found in the logarithmic time relaxation of J_c (flux creep).[4,15,30] In the inset of Fig. 2 we find that $S(T)$ is very similar for the YBCO and YGdBCO + BZO films at low T, consistent with the similar $J_c(H)$ (α values) observed at low temperatures. Despite the different values of J_c, both films exhibit the same $S(T)$ at low T and show a clear maximum near $T \sim 20$ K. The peak in $S(T)$ can be related to double kink expansion of the vortices from c-axis-correlated disorder.[4,28,30] Given the noncontinuous nature of the dislocations, the only source of correlated defects left in these films are TBs. This leads us to

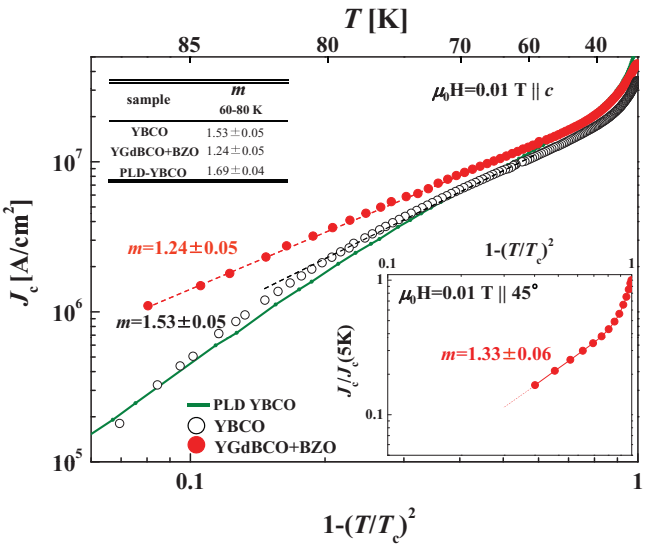

FIG. 4. (Color online) Log-log plot of J_c versus $[1-(T/T_c)^2]$ to show the temperature dependence at $\mu_0 H = 0.01$ T$\|c$ axis. For comparison, the data for a PLD-YBCO film are added. (Inset figure) Log-log plot of normalized J_c versus $[1-(T/T_c)^2]$ for the YGdBCO + BZO film at $\mu_0 H = 0.01$ T $\|$ 45°.

conclude that TBs work as c-axis-correlated disorder in both MOD films. Thus, it is clear that TBs and point defects coexist as dominant sources of pinning at low temperatures, again emphasizing the need for a deeper understanding of mixed landscapes and their possible synergistic effects. Finally, note that for $T > 40$ K a clear decrease in $S(T)$ is seen for the YGdBCO + BZO film with respect to that of the YBCO, consistent with the stronger pinning of the BZO nanoparticles at high T.

In type II superconductors, pinning results from spatial variations of the Ginzburg-Landau (GL) order parameter $|\psi|$; the spatial variation of $|\psi|$ can be associated with disorder in the T_c and/or from spatial variations in the charge carrier mean free path l near lattice defects.[28] These two kinds of pinning are called "δT_c" and "δl" pinning, respectively. In both cases J_c can be described as $J_c(T/T_c) \propto [1-(T/T_c)^2]^m$. For single vortex pinning, the characteristic exponent $m = 1.2$ holds for δT_c pinning and 2.5 holds for δl pinning.[31]

In Fig. 4, we present the J_c versus $[1-(T/T_c)^2]$ in the single vortex regime (μ_0H = 0.01 T $\|c$) for both YBCO and YGdBCO + BZO films. In Fig. 4 two regimes can be seen, above and below 40 K. For $T < 40$ K both samples have very similar temperature dependencies, while for $T > 40$ K clear differences arise. The YBCO film shows $m = 1.53 \pm 0.05$ and a rapid decay of J_c for $T > 83$ K. The value of $m = 1.53 \pm 0.05$ is close to the theoretical value for δT_c pinning. In the case of the YGdBCO + BZO film, $m = 1.24 \pm 0.04$ is also indicative of δT_c pinning, but no rapid decrease in J_c is seen at higher temperatures. We find that the rapid J_c decay for YBCO at high T moves to lower temperatures as the magnetic field is increased. In the case of the BZO-doped MOD film this drop off of J_c at high T is also observed but only at fields above 1 T. From these results, we find that δT_c pinning at $T > 40$ K for the YBCO film is consistent with the presence of the large $RE_2Cu_2O_5$ precipitates. However, as the temperature increases a more rapid decrease in J_c is found due to the effects of fluctuations. δT_c pinning for the YGdBCO + BZO film is also expected due to the presence of the insulating BZO nanoparticles.[12,32] The small but clear reduction of m at $T > 40$ K for the YGdBCO + BZO film as compared to the YBCO film (1.24 versus 1.53) is also consistent with the enhancement of J_c at high temperatures. For the YGdBCO + BZO film at $\mathbf{H}\|45°$ we found $m = 1.33 \pm 0.06$ (see inset of Fig. 4), again consistent with δT_c pinning. This value is very similar to the $\mathbf{H}\|c$ result and smaller than that of the YBCO for $\mathbf{H}\|c$. These results highlight the extended angular and temperature range of effectiveness that BZO nanoparticles have in increasing J_c in MOD films and are consistent with those observed by Gutiérrez *et al.*[10] and Puig *et al.*[33] For comparison, in Fig. 4 we have included the equivalent data for a PLD YBCO film. It also shows two different regimes below and above 40 K. For $T > 40$ K the data look qualitatively similar to those of the MOD YBCO film, with $m = 1.69 \pm 0.04$.

C. Irreversibility lines

We now focus on H_{irr}, where the vortex matter goes through a solid-liquid transition. H_{irr} is a key factor that determines the upper boundary of nonzero $J_c(H)$. Previously, we had investigated H_{c2} and H_{irr} at various angles for both MOD films (YGdBCO + BZO and YBCO) using pulsed fields up to 60 T.[34] From the H-T diagrams at various angles we found that H_{c2} is remarkably similar for both films in spite of their very different pinning landscapes. However, the changes in pinning landscape do influence H_{irr}, as a clear increase was found for the $H_{irr}(45°)$ up to 60 T of the YGdBCO + BZO with respect to YBCO.

Although a description of H_{irr} as $H_{irr} = A(T - T_c)^\beta$ (with A and β being constants) is a good approximation, closer examination of H_{irr} shows that if a good fit is obtained for $\mu_0 H > 20$ T, this fitting underestimates H_{irr} for the YGdBCO + BZO and overestimates H_{irr} for YBCO. This indicates that such a fit fails to describe H_{irr} in the entire temperature range correctly. An alternative approach is to plot H_{irr} as a function of $[1-(T/T_c)^2]$ on a log-log scale. This allows a better observation of regime changes, as well as the determination of the power law coefficient n (the slope in the log-log plot) in the different regimes.

Figure 5 shows plots of H_{irr} versus $[1-(T/T_c)^2]$ at various angles for the MOD YBCO, YGdBCO, and YGdBCO + BZO films. In all cases we observe a better fit to H_{irr}. For the MOD YBCO and YGdBCO + BZO films results for both pulsed and DC fields are included; the excellent agreement between data obtained by both methods confirms the consistency of both H_{irr} determinations as we had found in our previous studies.[34] As an additional confirmation of the independence of H_{irr} from the magnetic field sweep rate we repeated a few pulsed field measurements changing the maximum field, and consequently the field rate, and we found no variations. We first note that the H_{irr} for the MOD YBCO and YGdBCO films are almost identical, with exponents n that coincide within their errors, as indicated in Figs. 5(a) and 5(b), which supports the already-mentioned conclusion that the pinning mechanisms are similar. The MOD YBCO and YGdBCO + BZO films

show a clear change in the slope of H_{irr} versus $[1-(T/T_c)^2]$ around 65 K, 15 T for $\mathbf{H}\|c$ and $\mathbf{H}\|45°$. For $T \geqslant 65$ K, H_{irr} is clearly higher for the YGdBCO + BZO film than for the YBCO and YGdBCO films, both for $\mathbf{H}\|c$ and $\mathbf{H}\|45°$, with an exponent n consistently smaller. The values observed for n are 1.18 ± 0.09 and 1.26 ± 0.1 for YGdBCO + BZO ($\mathbf{H}\|$c and $\mathbf{H}\|45°$, respectively) and 1.45 ± 0.1 and 1.6 ± 0.08 for YBCO ($\mathbf{H}\|c$ and $\mathbf{H}\|45°$, respectively). For $T < 65$ K ($\mu_0 H > 15$ T) we find a very similar slope for both YGdBCO + BZO and YBCO with $n \sim 1.68$–1.8 for $\mathbf{H}\|c$ and $n \sim 1.85$–1.88 for $\mathbf{H}\|45°$, showing a common behavior for both orientations. Also included in Fig. 5 are the data for a PLD YBCO film.[35] For $\mathbf{H}\|c$ and $\mathbf{H}\|45°$ it exhibits a very similar behavior to that of the MOD YBCO film, consistent with the response found for $J_c(T)$.

For $\mathbf{H}\|ab$ we observe the same temperature dependence for MOD YBCO and YGdBCO + BZO samples with the same slope $n = 1.42$–1.43 up to the highest field measured (65 T). For this orientation the H_{irr} of the PLD film is higher than H_{irr} for the MOD films, with $n = 1.33 \pm 0.09$. However, it should be noted that in that case the film was better aligned along the *ab* planes using a rotating sample holder.[35]

Although this is not very apparent on the logarithmic scales of Fig. 5, for $\mathbf{H}\|c$ and $\mathbf{H}\|45°$ the addition of the BZO nanoparticles enhances H_{irr} at all temperatures, the effect being more pronounced for $\mathbf{H}\|45°$. However, the similar temperature dependence found for YBCO and YGdBCO + BZO for $T <$ 65 K ($\mu_0 H > 15$ T) indicates a less active role on the part of the BZO nanoparticles in that regime, not significant enough to determine the temperature dependence. Understanding the physical origin of the change of regime at $T \sim 65$ K and $\mu_0 H \sim 15$ T will require further studies. For $\mu_0 H \sim 15$ T the intervortex distance is $a_f \sim 10$ nm, smaller than the characteristic distances between BZO nanoparticles (~60 nm) or between TBs (~34 nm) but still of the same order of magnitude. Investigations on films with different amounts of BZO are underway and will help to elucidate this point.

D. Relationship between $J_c(T)$ and $H_{irr}(T)$

In general, we have seen the clear effect of the BZO addition on the superconducting properties of the films. Also, we have observed changes both in $J_c(T)$ and $H_{irr}(T)$ begging the question about a possible relationship between $J_c(T)$ and $H_{irr}(T)$. *A priori* there is no theoretical basis for a relation between these two quantities, but in a case where evidently there is a dominant pinning center this is a possibility worth studying. Attempts have been made to link the $J_c(T)$ and $H_{irr}(T)$, and a common mechanism was proposed by Matsushita.[36–39] According to that analysis, if $H_{irr} \propto [1-(T/T_c)^2]^n$ and $J_c(T/T_c) \propto [1-(T/T_c)^2]^m$ in the single vortex regime, and $J_c \propto B^{-\alpha}$, then $n = 2m/(1+2\alpha)$. If the same type of defect dominates $J_c(H,T)$ and H_{irr}, in principle the results for $J_c(T)$ could lead to a value for $H_{irr}(T)$. For the YBCO we found that $m = 1.53 \pm 0.05$ and $\alpha \sim 0.64$, leading to $n = 1.34$. Indeed, this is good agreement with $n = 1.45 \pm 0.1$ seen in Fig. 5. However, this fails to account for the change in slope (to $n = 1.8 \pm 0.04$) observed for $T < 65$ K. For the YGdBCO + BZO we face the lack of a clear α at high temperatures ($T = 65$ and 75 K), but as a first approximation we note that n is proportional to m and that the same relation

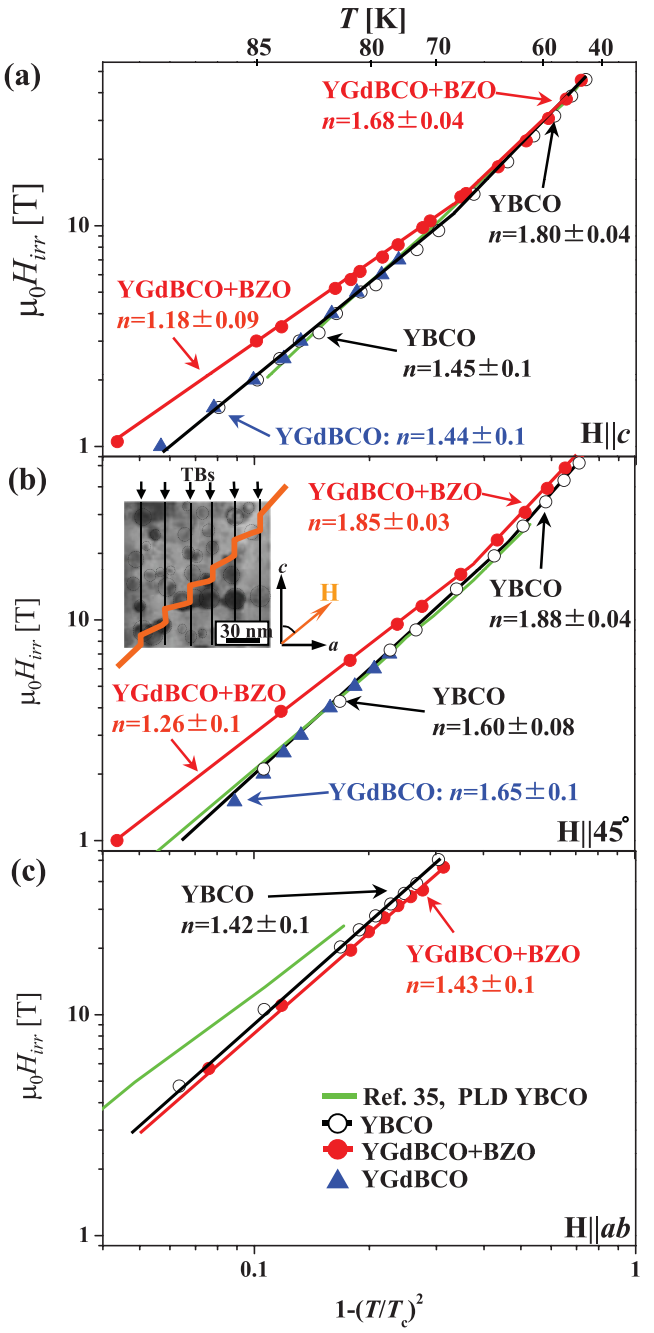

FIG. 5. (Color online) Log-log plot of H_{irr} vs $[1-(T/T_c)^2]$ at various angles for YBCO (open circles) and YGdBCO + BZO (solid circles) films at $\mathbf{H}\|c$, $\mathbf{H}\|45°$, and $\mathbf{H}\|ab$. For comparison, H_{irr} for MOD YGdBCO (solid triangles, Ref. 18) and PLD YBCO (solid line, Ref. 35) films are plotted. Right inset of (b): The zigzagging line represents a possible configuration of a vortex pinned by *c*-axis correlated TBs (vertical lines) and BZO nanoparticles.

is observed in n and m between YGdBCO + BZO and YBCO. Although Matsushita's model does not take into account the fact that H_{irr} changes for $T < 65$ K, it does reflect the correlation between n and m in the higher temperature region. By analyzing the experimental exponents [m, α and n] in the $J_c(T)$, $J_c(B)$ and $H_{irr}(T)$ curves we can clearly determine the regions where the nanoparticles are most effective and where

these exponents for the YGdBCO + BZO film differ from those found for the MOD-YBCO and the PLD-YBCO films. By controlling the mixed pinning landscape resulting from a combination of *c*-axis-correlated TBs and strongly pinning nanoparticles, we believe further enhancements in J_c and H_{irr} can be obtained for the REBCO films.

IV. SUMMARY

In summary, we have demonstrated significant enhancement of flux pinning up to 60 T through a control of size and distribution of disorder in the REBCO films. All of the $J_c - T, J_c - B$, and $H_{irr} - T$ relations clearly indicate that the YGdBCO + BZO film shows a higher and improved J_c and H_{irr} than those for the YBCO film and a more isotropic pinning dependence. We also found a correlation in the exponents [m, α, and n] with the BZO nanoparticle addition, especially at high temperatures. In particular, a clear trend between m and n can be established at high temperatures, with some limitations. The understanding of the effect on flux pinning of the mixed pinning landscapes resulting from a combination of various dimensional disorder is important and required for further improvement of in-field properties.

ACKNOWLEDGMENTS

We thank T. Kato for assistance with TEM observations. This work was supported by the Laboratory Directed Research and Development program at Los Alamos National Laboratory (M.M.); by the US DOE, Office of Basic Energy Sciences, Materials Sciences and Engineering Division (B.M., N.H., L.C.); by NHMFL-UCGP, the State of Florida, and the US NSF (S.A.B.). Work at ISTEC-SRL was supported by NEDO as a Collaborative Research (T.I., Y.S.).

*miura38ktgaj@gmail.com

[1] M. Paranthaman and T. Izumi, MRS Bulletin. **29**, 533 (2004).
[2] S.R. Foltyn, L. Civale, J. L. Macmanus-Driscoll, Q. X. Jia, B. Maiorov, H. Wang and M. Maley, Nat. Mat. **6**, 631 (2007).
[3] M. P. A. Fisher, Phys. Rev. Lett. **62**, 1415 (1989); D. R. Nelson and V. M. Vinokur, Phys. Rev. Lett. **68**, 2398 (1992); M. V. Feigel'man, V. B. Geshkenbein, A. I. Larkin, and V. M. Vinokur, Phys. Rev. Lett. **63**, 2303 (1989).
[4] L. Civale, A. D. Marwick, M. W. McElfresh, T. K. Worthington, A. P. Malozemoff, F. H. Holtzberg, J. R. Thompson, and M. A. Kirk, Phys. Rev. Lett. **65**, 1164 (1990).
[5] L. Civale, A. D. Marwick, T. K. Worthington, M. A. Kirk, J. R. Thompson, L. Krusin-Elbaum, Y. Sun, J. R. Clem, and F. Holtzberg, Phys. Rev. Lett. **67**, 648 (1991).
[6] M. Murakami, Mod. Phys. Lett. B **4**, 163 (1990).
[7] F. Sandiumenge, B. Martinez, and X. Obradors, Supercond. Sci. Technol. **10**, A93 (1997).
[8] C. J. van der Beek, M. Konczykowski, A. Abal'ochev, I. Abalosheva, P. Gierlowski, S. J. Lewandowski, M. V. Indenbom, and S. Barbanera, Phys. Rev. B **66**, 024523 (2002).
[9] J. Gutiérrez *et al*., Nat. Mat. **6**, 367 (2007).
[10] V. F. Solovyov *et al*., Supercond. Sci. Tech. **20**, L20 (2007).
[11] A. O. Ijaduola, J. R. Thomposon, R. Feenstra, D. K. Christen, A. A. Gapud, and X. Song, Phys. Rev. B **73**, 134502 (2006).
[12] T. G. Holesinger *et al.,* Adv. Mater. **20**, 391 (2008).
[13] A. E. Koshelev (unpublished).
[14] A. Gurevich, in *US DOE 2010 Advanced Cables and Conductors Program Peer Review* [http://www.htspeerreview.com/pdfs/presentations/day 2/strategic-research/1_SR_CurrentLimitingMechanismStudiesofCoatedConductors.pdf].
[15] B. Maiorov, S. A. Baily, H. Zhou, O. Ugurlu, J. A. Kennison, P. C. Dowden, T. G. Holesinger, S. R. Foltyn, and L. Civale, Nat. Mat. **8**, 398 (2009).
[16] J. Hua, U. Welp, J. Schlueter, A. Kayani, Z. L. Xiao, G. W. Crabtree, and W. K. Kwok, Phys. Rev. B **82**, 024505 (2010).
[17] Y. Yamada, S. Miyata, M. Yoshizumi, H. Fukushima, A. Ibi, A. Kinoshita, T. Izumi, Y. Shiohara, T. Kato and T. Hirayama, IEEE Trans. Appl. Supercond. **19**, 3236 (2009).
[18] M. Miura, T. Kato, M. Yoshizumi, Y. Yamada, T. Izumi, Y. Shiohara, and T. Hirayama, Appl. Phys. Express **2**, 023002 (2009).
[19] C. L. Johnson, J. K. Bording, and Y. Zhu, Phys. Rev. B **78**, 014517 (2008).
[20] J. L. Macmanus-Driscoll, S. R. Foltyn, Q. X. Jia, H. Wang, A. Serquis, L. Civale, B. Maiorov, M. E. Hawley, M. P. Maley and D. E. Peterson, Nat. Mat. **3**, 439 (2004).
[21] S. Kang, A. Goyal, J. Li, A. A. Gapud, P. M. Martin, L. Heatherly, J. R. Thompson, D. K. Christen, F. A. List, M. Paranthaman, and D. F. Lee, Science **311**, 1911 (2006).
[22] Y. Yamada *et al*., Appl. Phys. Lett. **87,** 132502 (2005).
[23] M. Miura, Y. Yoshida, Y. Ichino, Y. Takai, K. Matsumoto, A. Ichinose, S. Horii, and M. Mukaida, Jpn. J. Appl. Phys. **45**, L11 (2006).
[24] M. Miura, M. Yoshizumi, T. Izumi, and Y. Shiohara, Supercond. Sci. Technol. **23**, 014013 (2010).
[25] B. Maiorov and L. Civale, *Flux Pinning and AC Loss Studies on YBCO Coated Conductors,* Edited by M. P. Paranthaman and V. Selvamanickam (Nova Science, Hauppauge, NY, 2007).
[26] J. R. Thompson, O. Polat, D. K. Christen, D. Kumar, P. M. Martin, and J. W. Sinclar, Appl. Phys. Lett. **93**, 042506 (2008).
[27] J. Plain, T. Puig, F. Sandiumenge, X. Obradors, and J. Rabier, Phys. Rev. B **65**, 104526 (2002).
[28] G. Blatter, M. V. Feigelman, V. B. Geshkenbein, A. I. Larkin, and V. M. Vinokur, Rev. Mod. Phys. **66**, 1125 (1994).
[29] D. R. Nelson, *Defects and Geometry in Condensed Matter Physics* (Cambridge University Press, Cambridge, UK, 2002).
[30] J. R. Thompson, L. Krusin-Elbaum, L. Civale, G. Blatter, and C. Feild, Phys. Rev. Lett. **78**, 3181 (1997).
[31] R. Griessen, Wen. Hai-hu, A. J. J. van Dalen, B. Dam, J. Rector, H. G. Schnack, S. Libbrecht, E. Osquiguil, and Y. Bruynseraede, Phys. Rev. Lett. **72**, 1910 (1994).
[32] T. Aytug *et al*., Phys. Rev. B **74**, 184505 (2006).
[33] T. Puig, J. Gutierrez, A. Pomar, A. Llordes, J. Gazquez, S. Ricart, F. Sandiumenge, and X. Obradors, Supercond. Sci. Technol. **21**, 34008 (2008).

[34]M. Miura, S. A. Baily, B. Maiorov, L. Civale, J. O. Willis, K. Marken, T. Izumi, K. Tanabe and Y. Shiohara, Appl. Phys. Lett. **96**, 072506 (2010).
[35]S. A. Baily, B. Maiorov, H. Zhou, F. F. Balakirev, M. Jaime, S. R. Foltyn and L. Civale, Phys. Rev. Lett. **100**, 027004 (2008).
[36]T. Matsushita, E. S. Otabe, B. Ni, and K. Kimura, Jpn. J Appl. Phys. **30**, L342 (1991)
[37]T. Matsushita, E. S. Otabe, M. Kiuchi, B. Ni, T. Hikata, and K. Sato, Physica C **201**, 151 (1992).
[38]T. Matsushita, E. S. Otabe, T. Fukunaga, K. Kuga, K. Yamafuji, K. Kimura and M. Hashimoto, IEEE. Trans. Appl. Suppercond. **3**, 1045 (1993).
[39]T. Matsushita, T. Fujiyoshi, K. Toko and K. Yamafuji, Appl. Phys. Lett. **45**, 2039 (1990).